Analysis and simulation of BGK electron holes

L. Muschietti, I. Roth, R. E. Ergun, and C. W. Carlson

Space Sciences Laboratory, University of California, Berkeley, CA 94720, USA

Abstract. Recent observations from satellites crossing regions of magnetic-field-aligned electron streams reveal solitary potential structures that move at speeds much greater than the ion acoustic/thermal velocity. The structures appear as positive potential pulses rapidly drifting along the magnetic field, and are electrostatic in their rest frame. We interpret them as BGK electron holes supported by a drifting population of trapped electrons. Using Laplace transforms, we analyse the behavior of one phase-space electron hole. The resulting potential shapes and electron distribution functions are self-consistent and compatible with the field and particle data associated with the observed pulses. In particular, the spatial width increases with increasing amplitude. The stability of the analytic solution is tested by means of a two-dimensional particle-in-cell simulation code with open boundaries. We consider a strongly magnetized parameter regime in which the bounce frequency of the trapped electrons is much less than their gyrofrequency. Our investigation includes the influence of the ions, which in the frame of the hole appear as an incident beam, and impinge on the BGK potential with considerable energy. The nonlinear structure is remarkably resilient.

1 Introduction

As a new generation of satellites explore the magnetosphere with instruments faster at measuring electromagnetic fields, a growing body of observations report the presence of rapidly-moving solitary potentials. The structures have the electromagnetic signature of a positive charge surrounded by a negative cloud. They appear as positive potential pulses that move along the ambient magnetic field with speeds substantially greater than the ion acoustic velocity. Due to these space observations, phase-space electron holes have recently garnered a lot of interest (Omura et al., 1996; Krasovsky et al., 1997; Miyake et al., 1998; Goldman et al., 1998; Muschi-

etti et al., 1999a). The topic had hitherto been investigated in some specialized laboratory plasma experiments (Saeki et al., 1979; Lynov et al., 1979), in early computer simulations of the two-stream instability (Morse and Nielson, 1969; Berk et al., 1970), and in analytical detail for a special class of electron holes (Schamel, 1979, 1982; Korn and Schamel, 1995).

So far, the best space data have been collected by the FAST satellite and its high-resolution plasma and field instruments in the downward-current regions of the auroral zone. The observed potential structures (Ergun et al., 1998a) can have a large enough amplitude (~ 100 Volts) to modulate the entire electron distribution function ($e\Phi \sim T_e$) and have a parallel size of a few Debye lengths. Moving along the magnetic field opposite to the current with a speed on the order of the electron drift, they create a bipolar electric signal with amplitudes typically ~ 100 mV/m.

Similar solitary structures have been observed at higher altitudes in the auroral zone by the POLAR satellite. There are reports of observations at 2 R_E (Mozer et al., 1997; Bounds et al., 1999) as well as at 5–7 R_E (Franz et al., 1998; Cattell et al., 1999). In the plasma sheet boundary layer at large distances into the magnetotail, the GEOTAIL satellite has measured similar potential spikes, albeit with a smaller associated electric field (~ 0.1 mV/m). The spikes were identified as the components of the broadband electrostatic noise (Matsumoto et al., 1994; Omura et al., 1996). Finally, convective, positive potential pulses have also been reported at bow shock crossings by the WIND satellite, and interpreted as possible electron holes (Bale et al., 1998).

In analysing a nonlinear solitary wave it is customary to distinguish between the particles which are trapped in the frame of the wave, or interact strongly with the latter, and those which just pass it and interact weakly. Even the FAST satellite cannot measure a full particle distribution in the short time (0.1 ms) when a potential spike passes by. The measurements, however, reflect well the characteristics of the passing electrons. The distributions are drifting and broad in the direction parallel to the magnetic field with a flat-top (Carlson

---

Correspondence to: L. Muschietti

et al., 1998). By contrast, the information about the trapped electrons is much less clear. Cuts in the distributions, available on a much shorter time scale, display strong modulations at the passage of a potential spike. These modulations can be interpreted as a brief broadening accompanied by a decrease in the flat-top.

The plasma environment of the spikes observed by FAST is collisionless and characterized by a markedly low density. This results in a ratio gyro-to-plasma frequency $\Omega_e/\omega_e \sim 5$–15 and a rather large Debye length of order 100 m. Because the electrons are tightly tied to a magnetic field line, their one-dimensional dynamics is what mainly determines the observed potential spike.

In Sect. 2 a one-dimensional BGK solution (Bernstein et al., 1957; Turikov, 1984) is constructed which displays the characteristics of the observed potential and electron distribution. Its stability is tested in Sect. 3 by loading it as initial condition in a particle-in-cell (PIC) code. Our simulation code is two-dimensional, electrostatic, and designed with mixed open and periodic boundaries (Sect. 3.1). We carry out the simulations in the frame of the spike and investigate also the influence of the ions (Sect. 3.3). Some of the results have been recently published in the short form of a Letter (Muschietti et al., 1999a).

2 Localized BGK electron hole

Following the BGK scheme we assume that there exists a frame in which both potential and electron distribution are in a self-consistent steady state. Working in this frame, we write the electron distribution function in terms of the normalized constant of motion $w \equiv v^2 - \phi$ to satisfy the stationary Vlasov equation. The constant of motion w is twice the energy of an electron with mass m and charge $-e$ while $\phi(x)$ denotes the normalized potential profile along the ambient magnetic field. One uses the standard dimensionless units where length is normalized by the Debye length λ_d and velocity is normalized by the electron thermal velocity $v_e \equiv \sqrt{T_e/m} = \omega_e/\lambda_d$. In these units $\phi(x)$ is normalized by $T_e/2e$.

Let $f_t(w)$, $f_e(w)$, be the distribution functions of respectively the trapped and the passing electrons. Due to the hypothesis of steadiness the trapped electrons must be symmetric with the same flux of right and left moving particles in phase space. By contrast, the passing electrons need not have that symmetry and split into $f_e^+(w) + f_e^-(w)$. Poisson equation can be rewritten as

$$\int_{-\phi}^{0} \frac{f_t(w)}{(w+\phi)^{1/2}} dw = \frac{1}{2}\frac{d^2\phi}{dx^2} + 1$$
$$- \int_{0}^{\infty} \frac{f_e^+(w) + f_e^-(w)}{2(w+\phi)^{1/2}} dw. \quad (1)$$

The terms on the RHS are supposedly known by properly modelling the observations from the FAST satellite. The second term on the first line (+1) represents the ions, which we

assume to be unaffected for the moment and to create only a neutralizing background. By contrast, the LHS is virtually unknown, save for a few hints in the particle data. We formally define it as an unknown function of ϕ,

$$n_t(\phi) \equiv \int_{-\phi}^{0} \frac{f_t(w)}{(w+\phi)^{1/2}} dw . \quad (2)$$

Note that $n_t(\phi)$ is the density of trapped electrons expressed as a function of the potential profile. Our aim is not only to obtain this density but also to solve explicitly for the detailed distribution function $f_t(w)$, the expression of which will be used in Sect. 3 to load the particles in the PIC simulation code. From (1) it is clear that there are two contributions to $n_t(\phi)$: one is the net density perturbation required by the shape of the potential, $n_s(\phi) \equiv \frac{1}{2}d^2\phi/dx^2$, the other is the density of passing electrons, $n_p(\phi) \equiv \int_{0}^{\infty} \frac{1}{2}[f_e^+(w) + f_e^-(w)](w+\phi)^{-1/2}dw$, a density which naturally decreases as these electrons are accelerated about the potential spike. The two contributions,

$$n_t(\phi) = n_s(\phi) - n_p(\phi) + 1 , \quad (3)$$

are straightforward to evaluate for given models of potential profile $\phi(x)$ and passing electrons $f_e^+(w), f_e^-(w)$.

2.1 Potential profile

After analysing several hundreds of the rapidly-moving potential spikes from the FAST dataset, it was concluded (Ergun et al., 1998b) that a Gaussian provides a reasonably good fit to their spatial profile in the parallel direction. We therefore introduce the following ansatz,

$$\phi(x) = \psi \exp(-0.5\, x^2/\Delta^2) , \quad (4)$$

which results in

$$n_s(\phi) = \frac{\phi}{2\Delta^2}\left[2\ln(\frac{\psi}{\phi}) - 1\right] \quad \text{with} \quad 0 \le \phi \le \psi. \quad (5)$$

Where $\phi \lesssim \psi$, the term above is negative: there must be a dearth of electrons at the center of the spike. A numerical value of 5% is typical for our model and the FAST data. Where $\phi < \psi e^{-0.5}$ (or $|x| > \delta$) there is a surplus of electrons screening the positive charge left in the center.

2.2 Passing electrons

The electron distributions measured by the FAST satellite in regions of solitary spikes are drifting and broad in the parallel direction; they are flat-topped and drop beyond a certain energy (Carlson et al., 1998; Ergun et al., 1998b). Because the compilation of a full electron distribution takes $\sim$80 ms while a potential spike moves by the satellite in just 0.1 ms, these measurements are an average that reflects mostly the characteristics of the electrons in-between the spikes, namely the passing electrons. In the satellite frame the electron distributions appear to have an average drift larger or comparable to the velocity of the spikes (Ergun et al., 1998b). Hence, we

shall assume the electron drift to be zero in the frame of the potential spike. Furthermore, for simplicity we shall assume that the distributions are symmetric, $f_e^+(w) = f_e^-(w) = f_e(w)$, and introduce the following model. Though somewhat arbitrary, it qualitatively emulates the data and keeps the calculations simple:

$$f_e(w) = \frac{6\sqrt{2}}{\pi(8+w^3)} \quad \text{with } w > 0. \tag{6}$$

Using (6) to integrate $n_p(\phi)$ (third term in the RHS of (1)) for a position where $\phi = 0$, one may check that the density is normalized to unity, which cancels exactly the ion contribution. The "temperature", or spread, $2\int_0^\infty dv\, v^2 f_e(v^2)$, is also normalized to unity. An electron with $w = v^2 = 1$ is a "thermal" electron (in the spike frame). For smaller energies $f_e(w)$ is flat, while it drops as a power-law for larger energies.

On physical grounds it is expected that the density of passing electrons decreases in the vicinity of the potential spike as they are accelerated by the positive potential. Unfortunately, there is no simple explicit expression for $n_p(\phi)$ that can be obtained using (6) in the integrand. One can, however, after an integration by parts which brings a term in $\sqrt{\phi}$, write down the first terms of an expansion for small ϕ:

$$n_p(\phi) = 1 - \frac{3\sqrt{\phi}}{\sqrt{2\pi}} + \frac{\phi}{4} - \frac{3\phi^2}{64} + O(\phi^3). \tag{7}$$

While the expansion also includes a linear and quadratic response of the passing electrons, the main one is a reduction in density scaling as $\phi^{1/2}$. It is interesting to compare the expression above to equation (9) of Krasovsky et al. (1997), who studied the role of passing electrons for an unspecified distribution function. Using their notation we can rewrite (7) as

$$n_p(\phi) = 1 - 2f_0\phi^{1/2} - P\phi/2 + O(\phi^2) \tag{8}$$

where $f_0 = 3/(2\sqrt{2\pi})$ is the value of the distribution f_e at the separatrix, $w = 0$, and $P \equiv 2\int_0^\infty v^{-1}\frac{\partial}{\partial v}f_e(v^2)dv$. Since our ϕ is twice their ϕ due to different normalizations, the two expressions agree. The main reduction in density originates therefore from those passing electrons that move closely along the separatrix and are in some sense resonant (Krasovsky et al., 1997).

Fortunately, we need not use the approximate relation (7) for calculating the distribution function of trapped electrons. Instead, as we shall see in the next section, we can restart from (1) and manipulate the integral to obtain an exact expression that is valid for any amplitude of ϕ.

2.3 Trapped electrons

We now proceed to invert (2) for $f_t(w)$. Noting that the unknown function $f_t(w)$ is defined for $w < 0$ we introduce the auxiliary function $A(u)$ defined over the half space $u > 0$ such that $A(u) \equiv f_t(w = -u)$, and take the Laplace transform of (2). This yields $\mathcal{L}[n_t(\phi)] = \mathcal{L}[u^{-1/2}]\,\mathcal{L}[A(u)]$.
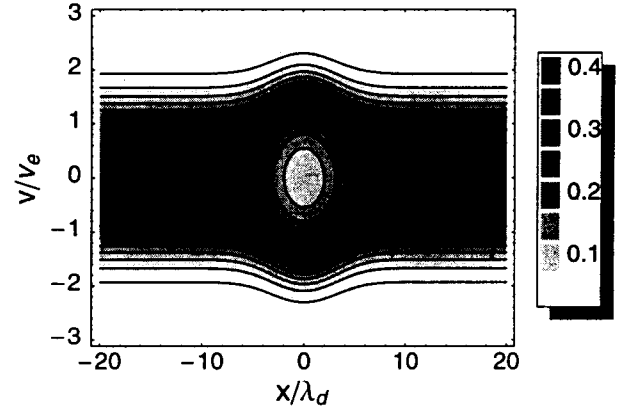

Fig. 1. Example of a distribution function exhibiting a BGK phase-space hole. Contours are linearly spaced with gray scale indicated on the bar. The plot is computed from (13) with dimensionless $\psi = 1.6$ and $\Delta = 3$. Note the phase space depletion about $x = 0$, center of the potential spike, and the flat-topped distribution at large $|x|$.

Therefore, using $\mathcal{L}[u^{-1/2}] = (-1/2)!s^{-1/2}$ as well as the relation $((-1/2)!)^2 = \pi$, one obtains in succession

$$\mathcal{L}[A(u)] = \frac{s^{1/2}}{(-1/2)!}\mathcal{L}[n_t(\phi)] = \frac{1}{\pi}\mathcal{L}[\phi^{-1/2}]\,s\mathcal{L}[n_t(\phi)]. \tag{9}$$

The term on the RHS is substituted with the transform of the derivative of $n_t(\phi)$ while using the property $n_t(\phi) = (n_s(\phi) - n_p(\phi) + 1) \to 0$ for $\phi \to 0_+$, which assumes neutrality away from the spike. One then takes the inverse Laplace transform and finally obtains the convolution integral:

$$f_t(w) = \frac{1}{\pi}\int_0^{-w} \frac{1}{\sqrt{-w-\phi}}\,\frac{d}{d\phi}n_t(\phi)\,d\phi. \tag{10}$$

The expression above can be integrated exactly for our model of potential profile and distribution of passing electrons. Substituting (5) for $n_s(\phi)$ and

$$n_p(\phi) = \frac{6\sqrt{2}}{\pi}\int_0^\infty \frac{1}{(w+\phi)^{1/2}(w^3+8)}dw \tag{11}$$

into (3), we obtain from (10)

$$\begin{aligned}
f_t(w) &= \frac{\sqrt{-w}}{\pi\Delta^2}\left[1 + 2\ln(\frac{\psi}{-4w})\right] \\
&+ \frac{6 + (\sqrt{2}+\sqrt{-w})(1-w)\sqrt{-w}}{\pi(\sqrt{2}+\sqrt{-w})(4-2w+w^2)} \\
&\quad \text{with } -\psi \le w < 0.
\end{aligned} \tag{12}$$

The term on the first line comes from $n_s(\phi)$. It is negative near the hole center $w \to -\psi$, becomes positive at the periphery, and vanishes for $w \to 0_-$. It reflects the requirement of net density perturbation between the hole center and the periphery that is imposed by the different curvatures of ϕ at its peak and on its flanks. The term is very sensitive to the width Δ. The term on the second line remains positive and is independent of Δ. It comes from the passing electrons whose density decrease about the positive potential needs be offset

by a contribution of trapped electrons. In the limit $w \to 0_-$ one has $f_t \to 3/(2\sqrt{2\pi})$, which matches continuously with the passing distribution f_e from (6). Fig. 1 provides an illustration of the complete distribution function in (x, v) space.

$$F(x, v) = \begin{cases} f_t(w = v^2 - \phi(x)), & \text{if } w < 0 \\ f_e(w = v^2 - \phi(x)), & \text{if } w > 0 \end{cases} \quad (13)$$

Considering F as a function of v, note how the distribution is strongly depleted around $x = 0$ where the solitary potential is centered, while flat-topped for positions away from it. Note also how F bulges where the potential is large. This feature is expected to translate into a brief broadening of the electron distributions observed in the spacecraft frame. In fact, cuts in the distributions recorded by the FAST satellite, which can be obtained on a much shorter timescale than the full distribution, reflect this broadening at times when a potential spike passes by.

2.4 Width-amplitude characteristics

Even though the solitary potential is due to a deficit of deeply trapped electrons, the trapped distribution f_t cannot be negative at its minimum for $w = -\psi$. This imposes a relation between width and amplitude. Substituting $w \to -\psi$ in (12) and balancing the term on the first line with that on the second, one finds

$$\Delta^2 \geq 4(4\ln 2 - 1)\sqrt{\Phi}(1 + \sqrt{\Phi})\frac{1 + \sqrt{\Phi} + \Phi}{3 + 4\sqrt{\Phi} + 2\Phi}. \quad (14)$$

Here, Δ, which is expressed in Debye units, is the half-width defined by (4) and Φ is the amplitude of the potential in usual T_e/e units. Clearly, $\Delta \sim \Phi^{1/4}$ for $\Phi \ll 1$ and $\Delta \sim \Phi^{1/2}$ for $\Phi \gg 1$. The width must increase for increasing amplitudes (Turikov, 1984).

Fig. 2 shows the boundary limit defined by (14) together with data points out of a statistical study of the FAST measurements (Ergun et al., 1998b). Over 1000 solitary potentials from 30 different orbits were binned by size. The size was defined as the Gaussian half-width normalized to the local Debye length while the amplitude was normalized to the local electron temperature. Nearly all data points lie to the right of the boundary curve showing good agreement. The behavior differs from that of a classic soliton, where the structures with the larger amplitudes are the narrower. An electron hole, and its associated solitary potential, is a different nonlinear structure for which the electrons trapped in a phase-space vortex play the dominant role. Interestingly, even ion-acoustic solitons may behave non-classically. In the wake of the Viking results, Berthomier et al. (1998) showed that there exist regimes in a two-electron temperature plasma where they can be refractive and display an anomalous relation between amplitudes, propagation velocities, and widths.

3 PIC simulations

The BGK scheme admits a wide variety of potential profiles and it is not *a priori* certain that the analytically con-
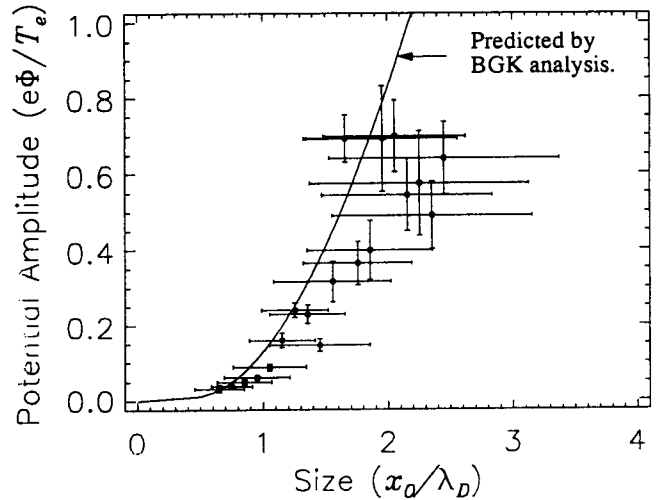

Fig. 2. Amplitude-width relation. Prediction from (14) is compared to data from the FAST satellite. Nearly all data points lie to the right of the boundary curve showing good agreement. Reproduced from Muschietti et al. (1999b).

structed electron hole is dynamically stable. Moreover, very early simulations of phase-space holes (or vortices) generated by the two-stream instability (Morse and Nielson, 1969), as well as analytical calculations (Schamel, 1982), suggested that the vortex structure disappears when phase-space is open to more than one spatial dimension. On the other hand, in the rarefied plasma of the mid-altitude auroral region where the solitary spikes are observed by FAST, the electrons are strongly magnetized and their motion restricted to the direction of the magnetic field, which may contribute to the stability of the electron hole. Recent two-dimensional simulations of phase-space vortices associated with the two-stream instability in a magnetized plasma (Goldman et al., 1998) show that they are stable for many plasma periods, yet emit electrostatic whistler waves at times $100 < \omega_e t < 1000$. Another two-dimensional simulation study (Miyake et al., 1998), in which a cold beam instability is used to generate the phase-space vortices, suggests that the ratio of the cyclotron frequency to the bounce frequency of the trapped electrons is a critical parameter for their stability.

Taking these considerations into account, we numerically investigate the stability and evolution of our analytical solution by performing a series of two-dimensional particle-in-cell (PIC) simulations. It is assumed that a potential spike with specific characteristics has been formed and co-exists with the populations of trapped and passing electrons as described in Sect. 2. We follow then the evolution of the potential as determined by the full dynamics of the particles in an open-boundary, electrostatic, PIC code. The simulation is carried out in the frame of the potential spike so as to follow the evolution over long times without the spike moving out of the simulation box. In the runs presented here, the cyclotron frequency is kept constant, $\Omega_e = 5\,\omega_e$. On the other hand, the bounce frequency associated with the potential model (4) is $\omega_B = \omega_e (e\psi/T_e)^{1/2}(\lambda_d/\Delta)$, which is of order $0.3\,\omega_e$.
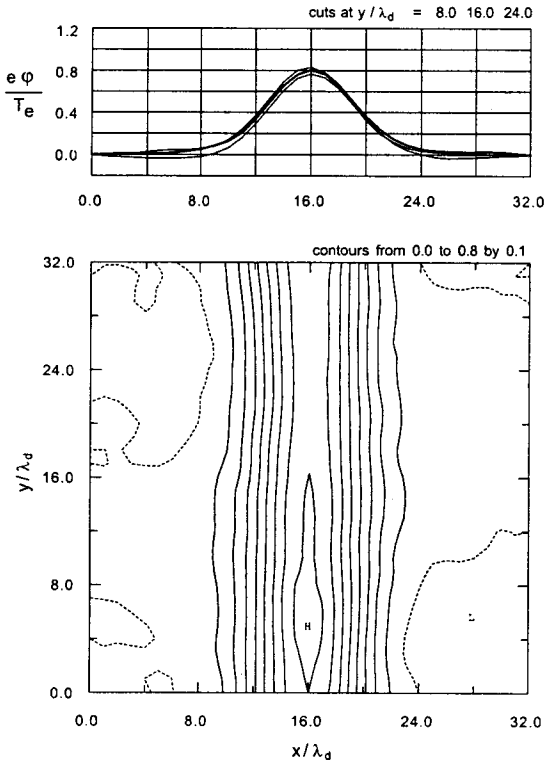
Fig. 3. Potential structure at $t = 0$ resulting from the inhomogeneous loading of the electrons in the PIC simulation. (Bottom) Nine contours from 0.0 (dotted) to 0.8 in (x, y) plane, where x is along the magnetic field. "H" and "L" refer to high and low, respectively. (Top) Three cuts at various y. Input parameters: $e\psi/T_e = 0.8$, $\Delta/\lambda_d = 3$.

Fig. 4. Potential structure recorded in the PIC simulation after 350 steps ($\omega_e t = 35$). (Bottom) Nine contours from 0.0 (dotted) to 0.8. "H" refers to high. (Top) Three cuts at different y are indistinguishable. Compare to Fig 3 and note the steadiness.

3.1 Open simulation system

Along the coordinate x, which describes the direction parallel to the magnetic field, we impose open boundary conditions. At both ends we inject populations of particles with a prescribed flux determined from $f_e(w = v_x^2)$ (see (6)), while exiting particles are removed from the system. The injection scheme uses sub-timesteps so as to spread the positions of the injected particles over the boundary cells. Due to losses and gains occurring at the boundaries, the total number of particles in the system is allowed to fluctuate in time. The resulting fluctuations in the potential at the boundaries are calculated from the current integrated over the whole simulation system. In the perpendicular direction y we impose periodic boundary conditions. As for initial conditions, electrons are loaded along x at $t = 0$ in a way that reproduces the spatially inhomogeneous function $F(w = v_x^2 - \phi(x))$ (see (6), (12), (13), and Fig. 1). Their spatial distribution in the y direction is given by a random, statistically homogeneous loading, while their distribution as a function of v_y and v_z is described by a narrow Maxwellian. Therefore, the profile of the potential has initially a dependence in x only, but it evolves in a two-dimensional simulation. We employ a large number of particles per Debye square (of order 2^{10}) for good diagnostic, to keep the noise level low, and, importantly, to ensure that many charges cross the box boundaries
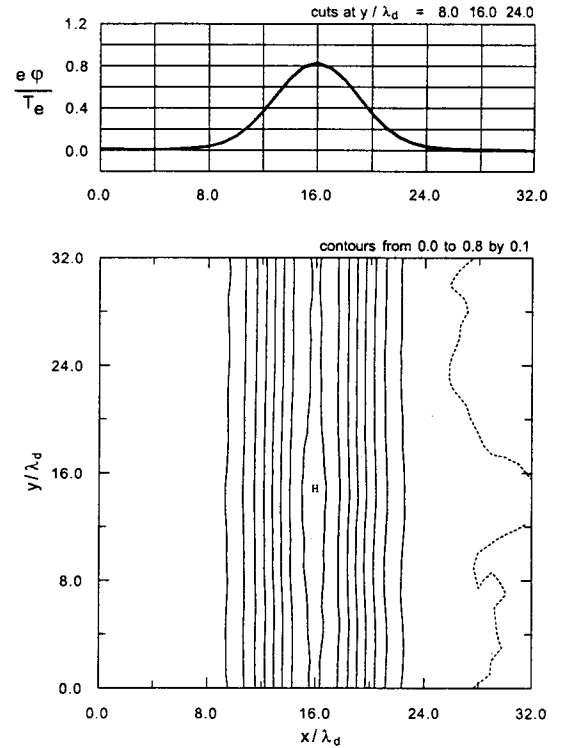
per timestep. The latter enables us to smoothen the injection process and limit the large fluctuations that the passage of discrete particles through the boundaries might create (see Muschietti et al. (1996) for details). Finally, the timestep $\omega_e \Delta t = 0.1$ is adequate to resolve the gyromotion of the electrons.

3.2 Simulations without mobile ions

Fig. 3 shows the potential structure created at $t = 0$ by our specific loading of the electron distribution function. The simulation box has dimensions $L_x \times L_y = 32\,\lambda_d \times 32\,\lambda_d$. The bottom panel gives the contours of the potential $\phi(x, y)$, while the upper panel shows cuts at three different locations $\phi(x, y_i)$ where $y_i = L_y/4$, $L_y/2$, $3L_y/4$. Except for irregularities associated with the random loading in the y direction, the potential profile has no y dependence and is described by (4) with $\Delta = 3\,\lambda_d$ and $e\psi/T_e = 0.8$. The ions form just a homogeneous background.

Fig. 4 displays the evolved potential after 350 steps ($\omega_e t = 35$). The steadiness is impressive. The potential structure remains one-dimensional and maintains very well its profile. The associated distribution function is shown in Figure 5, which is a snapshot taken from the simulation at $\omega_e t = 35$. Three spatial bins are examined: in a region left of the spike, in a region amidst the spike, and in a region right of the spike. Note the depleted distribution function of the center panel and the flat-topped distribution functions in the left and right
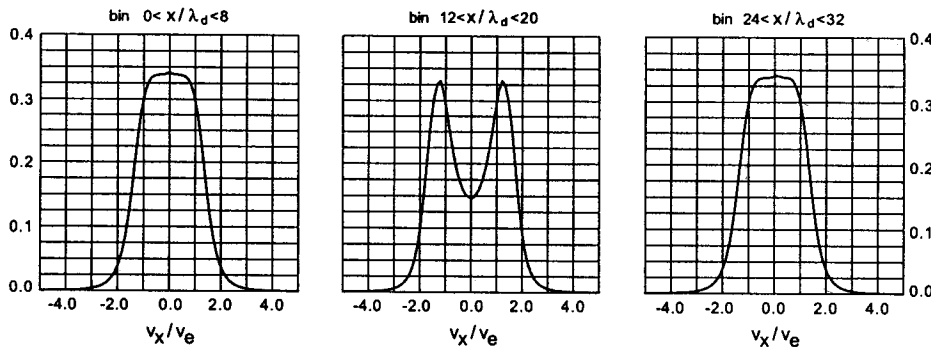
Fig. 5. Distribution functions associated with the potential shown in Fig. 4 ($\omega_e t$ =35). They are snapshots computed from the simulation with the help of three spatial bins. The central panel covers a distance $\sim \Delta$ on either side of the potential maximum at $x/\lambda_d = 16$. Note the excellent agreement with the analytical expectation (shown in Fig 1) for the depleted distribution: two maxima with values in excess of 0.3 located at $|v_x|/v_e > 1$ and a minimum with value below 0.2 about $v_x = 0$.

panels. From (13), or Fig. 1, one expects the value of F in the hole to be between 0.1 and 0.2. The agreement is thus excellent. Note also the symmetry between left and right moving electrons.

In order to eliminate the possible effects the boundaries might have on the spike, we enlarged the box to $128\lambda_d$ by $32\lambda_d$ and performed 10^3 steps with 4×10^6 particles reaching the time $\omega_e t = 100$. The input parameters were: $\Delta = 4\ \lambda_d$ and $e\psi/T_e = 1.0$. The result is displayed in Fig. 6, which again shows that the potential structure remains one-dimensional and maintains very well its profile.

Fig. 7 displays the contracted phase space of the electrons ($x - v_x$) associated with Fig. 6. All the electrons trapped initially (i.e. satisfying $w < 0$ at $t = 0$) have been tagged and are depicted separately in the upper panel at $\omega_e t = 100$. Similarly, the bottom panel shows all the electrons that were not trapped initially. With help of the current potential we calculate the separatrix ($w = 0$) between trapped and passing electrons, and show it as a solid line (replaced by null wherever the potential falls below rms fluctuations). Noteworthy are two points. First, because a typical electron should have moved $\sim 100\ \lambda_d$ since $t = 0$, the fact that the trapped electrons remain in a clump of $16\ \lambda_d$ demonstrates that the hole forms an entity by itself. Second, one may observe that a small fraction of the trapped electrons leaks through the separatrix whenever their velocity becomes small enough near the edges of the potential spike. These electrons are sensitive to random fluctuations in the background potential which can then push them through the separatrix. We should add that the small outflux of trapped electrons is balanced over time by a small influx of initially untrapped electrons which become trapped.

3.3 Simulations with mobile ions

The effects of the ions on the stability of the electron hole depend on their relative energy vs the potential energy of the spike. Since the observed potential spikes move with a velocity which is a sizeable fraction of the electron thermal speed, the ions appear in the frame of the spike as a cold beam impinging onto the solitary potential with considerable kinetic energy. Specifically, their energy w_i is $2 - 3$ orders of magnitude larger than that of a typical passing electron ($w \sim 1$). Therefore, in energy terms, the potential spike rep-
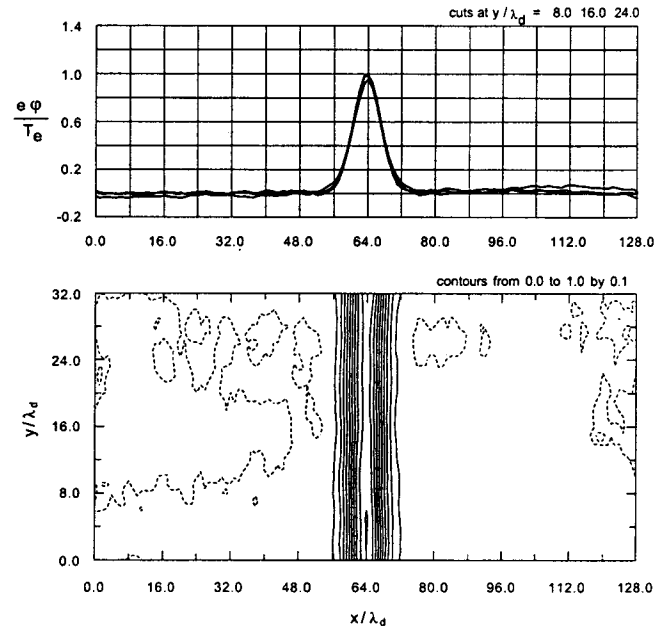

Fig. 6. Potential structure in a large simulation box after 1000 steps ($\omega_p t$ =100). (Bottom) Eleven contours from 0.0 (dotted) to 1. Beware the strechted aspect ratio. (Top) Three cuts at different y. Input parameters: $e\psi/T_e$ =1.0, Δ/λ_d =4.
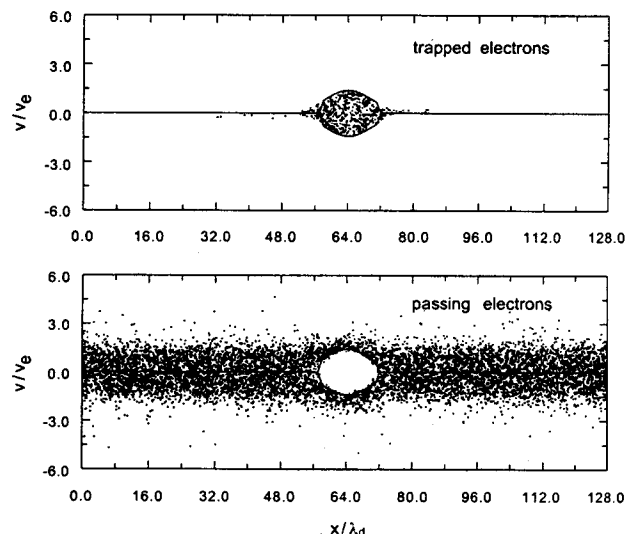

Fig. 7. Phase-space view of the electrons after 1000 steps ($\omega_e t$ =100). (Top) Electrons that were trapped at $t = 0$. (Bottom) Electrons that were untrapped at $t = 0$. The solid line shows the separatrix computed from the current value of the potential. See discussion in text.

resents only a small perturbation for the ions, which results in a brief and weak interaction. The opposite case, where the relative speed between the phase-space hole and the ions is on the order of the ion-acoustic speed, resulting in a strong interaction and a break-up of the electron hole into multiple sub-holes, has been studied by Saeki and Genma (1998).

There is no single way to initially load the ions, and their effect on the electron hole will depend upon which way one chooses. The results presented here are based on a homogeneous density of ions and a drifting velocity distribution that is function of the parallel energy, $w_i \equiv \frac{M}{2}v_x^2 + e\phi$ with M the ion mass. In the potential-free region, the ions drift relative to the electron hole with an average speed V_r and a velocity spread v_i. Their distribution as a function of the perpendicular velocities v_y and v_z is chosen to be a simple Maxwellian with thermal spread v_i.

As the ions flow over the potential hump, they slightly slow down on the upslope and accelerate on the downslope. This creates a density ripple leading to a perturbation of the electric field which acts upon the electron hole. We stress that the phenomenon is transient and associated with the initial conditions. Still, it interestingly perturbs and tests the stability of our constructed electron hole.

Fig. 8 displays five successive snapshots of the potential at $\omega_e t = 0, 10, 20, 30, 40$. Each panel includes three cuts at different y positions as in the upper panel of Fig. 3. Clearly, the main effect is a drift of the potential structure towards the right. In this run, ions with mass ratio $M/m = 100$ and velocity spread $v_i = 0.1\,v_e$ come from the right at a speed $V_r = -0.5\,v_e$. If the same ions come instead from the left boundary, the potential structure moves towards the left.

Let us analyse the process taking place. Since the ions appear as a cold beam in the hole frame, one treats them as fluid and, combining conservation of w_i and continuity equation, describes the perturbed ion density by

$$\partial_t n_i + V_r \partial_x n_i = -n_i \frac{e\psi}{MV_r} \frac{x}{\Delta^2} \exp(-0.5\,x^2/\Delta^2). \quad (15)$$

Since n_i has no spatial dependence initially, the advection term can be neglected during early times. Second, because we look for the perturbation δn_i, we replace n_i on the RHS with n_0 and obtain

$$\delta n_i(x,t) = n_0 \frac{e\psi}{MV_r} \frac{-x}{\Delta^2} \exp(-0.5\,x^2/\Delta^2)\,t \quad (16)$$

The perturbation is dipolar in space with extrema about $\pm\Delta$. Ions gather on the upslope of the potential hump and disperse on the downslope. The perturbed electric field associated with δn_i is

$$\delta E(x,t) = \omega_i^2 \frac{\psi}{V_r} \exp(-0.5\,x^2/\Delta^2)\,t \quad (17)$$

where ω_i^2 is the ion plasma frequency. The field, which maximizes at $x = 0$, has the sign of V_r and thus pushes the trapped electrons opposite to the incoming ions. As a result, the electron hole, which is supported by the trapped electrons, starts drifting against the incoming ions. From a
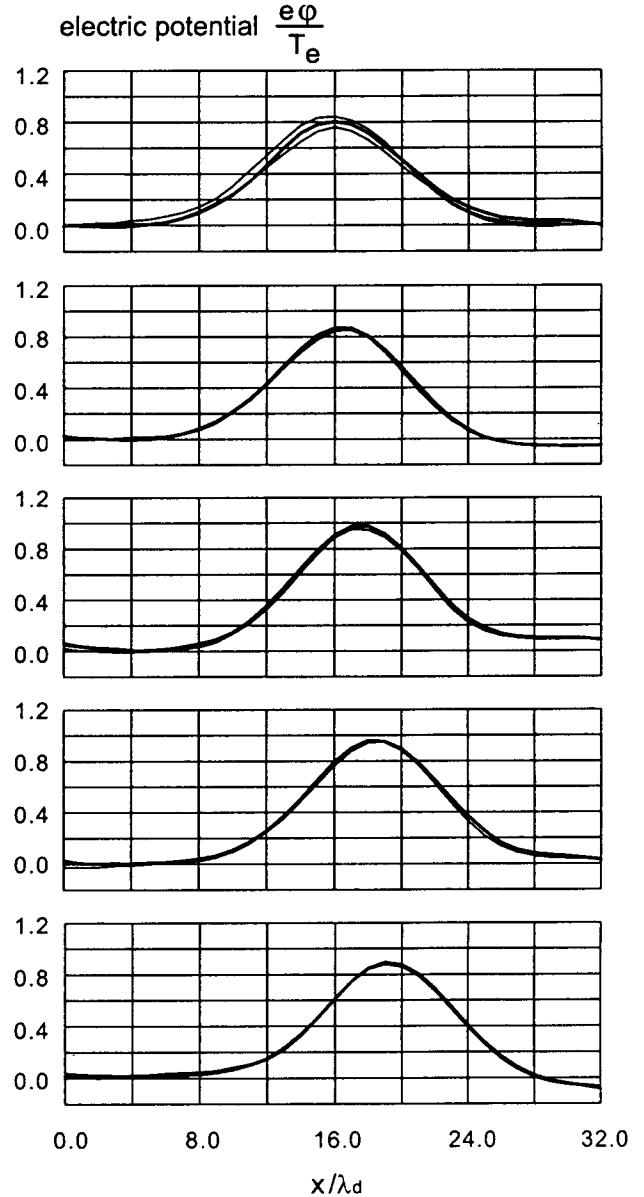

electric potential $\dfrac{e\varphi}{T_e}$

Fig. 8. Five successive snapshots of the potential structure in presence of ions coming from the right ($\omega_e t = 0, 10, 20, 30, 40$). Input parameters: $e\psi/T_e = 0.8$, $\Delta/\lambda_d = 4$, $M/m = 100$, $V_r/v_i = -0.5$. The main effect is a drift of the potential toward the incoming ions.
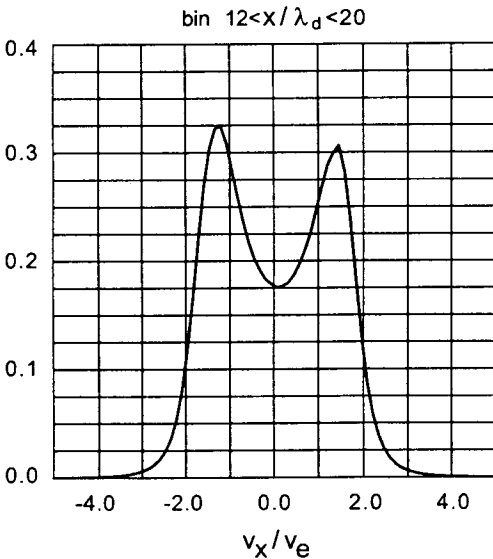
Fig. 9. Snapshot of the distribution function at $\omega_e t = 28$ during run shown in Fig 8. Compare with Fig 5 (case without ions) and note the asymmetry as well as the slight offset of the minimum toward $v_x > 0$. The trapped electrons are perturbed by the transient, dipolar electric field caused by the ions (see (17)).

macroscopic viewpoint it behaves as a positive structure with a negative mass. One should add that no growth of the hole (Korn and Schamel, 1995) is observed.

From a microscopic viewpoint one can find a signature of the interaction in the simulation by looking at the electron distribution functions recorded during the run. The snapshot displayed in Fig. 9 shows the asymmetry that develops in the distribution associated with the perturbed electron hole. Compare the plot to the central panel of Fig. 5 (case without ions) and note (with help of the background grid) the slight offset of the distribution toward positive velocities. The offset is noticeable in the concave portion of the curve, which pertains to the trapped electrons. We also notice that the right-moving electrons, which are accelerated by the perturbed electric field, have a lower density than the left-moving electrons, which are slowed down. After a short while, the peak of the drifting potential spike matches the location of the enhanced ion density, hence the dipolar, perturbed, electric field disappears and the ions reach a state where $n_i = n_0/[1 - \frac{m}{M}\phi/V_r^2]^{1/2}$. The whole structure thus appears to adjust to perturbations applied upon it and to be remarkably resilient.

4   Conclusion

We have constructed a BGK electron hole that displays the characteristics of the observed potentials and electron distributions. The profile of the solitary potential, which following the observations is a Gaussian with characteristic width and amplitude, is self-consistent with a plausible distribution function of electrons. The latter has two components. The passing, weakly interacting electrons are taken from the observations while the trapped, strongly interacting electrons

are deduced from Poisson equation. The expression for the distribution function is explicit and exact. It is valid for any amplitude of the potential and can be used in a particle-in-cell code.

Though it supports a solitary potential pulse, the electron hole is a nonlinear object different from a classic soliton. By tagging the trapped electrons in our simulations, we have demonstrated that it is an entity with an identity at the microscopic level. The solitary potential is associated with a clump of electrons trapped in a phase-space vortex and remaining so, unlike the potential of a soliton which is a fluid perturbation. Constructing the self-consistent distribution function enabled us to investigate the parametric dependence between amplitude and width. The existence curve indicates that amplitude and width must grow jointly, in contrast to a reverse dependence for a standard soliton.

The observations of isolated, localized potential spikes on several satellites indicate that the potential structures are stable over significant periods of time. In order to test the stability of the analytically constructed BGK hole, we have loaded it in a 2-D particle-in-cell simulation. The nonlinear structure is found to be very stable, in spite of the opening of phase space to a second dimension. The ions, in the frame of the hole, are incident and impinge on the solitary potential. Their influence is minor with regard to the stability, as long as their kinetic energy is large compared with the potential amplitude. Hence, the fast-moving potential spikes that have speeds on the order of the electron thermal velocity can be stable over significant periods of time.

References

Bale, S.D., Kellogg, P.J., Larson, D.E., Lin, R.P., Goetz, K., and Lepping, R.P., Bipolar electrostatic structures in the shock transition region: Evidence of electron phase space holes, *Geophys. Res. Lett.*, *25*, 2929–32, 1998.

Berk, H. L., Nielsen, C. E., and Roberts, K. V., Phase space hydronamics of equivalent nonlinear systems: experimental and computational observations, *Phys. Fluids, 13*, 980–995, 1970.

Bernstein, I. B., Greene J. M., and Kruskal M. D., Exact nonlinear plasma oscillations, *Phys. Rev., 108*, 546–550, 1957.

Berthomier, M., Pottelette R., and Malingre, M., Solitary waves and weak double layers in a two-electron temperature auroral plasma, *J. Geophys. Res., 103*, 4261–4270, 1998.

Bound, S.R., Pfaff, R.F., Knowlton, S.F., Mozer, F.S., Temerin, M.A., Kletzing, C.A., Solitary potential structures associated with ion and electron beams near 1 R_B altitude, *J. Geophys. Res. in press*, 1999.

Carlson, C.W., McFadden, J.P., Ergun, R.E., et al., FAST observations in the downward auroral current region: Energetic upgoing electron beams, parallel potential drops, and ion heating, *Geophys. Res. Lett., 25*, 2017–2020, 1998.

Cattell, C.A., Dombeck, J., Wygant, J.R., et al., Comparisons of Polar satellite observations of solitary wave velocities in the plasma sheet boundary and the high altitude cusp to those in the auroral zone, *Geophys. Res. Lett., 26*, 425–428, 1999.

Ergun, R.E., Carlson, C.W., McFadden, J.P., et al., FAST satellite observations of large-amplitude solitary structures *Geophys Res. Lett., 25*, 2041–2044, 1998a.

Ergun, R.E., Carlson, C.W., McFadden, J.P., et al., Debye-scale plasma structures associated with magnetic-field-aligned electric fields, *Phys. Rev. Lett., 81,* 826–829, 1998b.

Franz, J. R., Kintner, P. M., and Pickett, J. S., POLAR observations of coherent electric field structures, *Geophys. Res. Lett., 25,* 1277–1280, 1998.

Goldman, M. V., Oppenheim, M. M., and Newman, D. L., PIC simulations of bipolar wave structures driven by dense beams in the auroral ionosphere, in *Physics of Space Plasmas 15,* edited by T. Chang and J.R. Jasperse, p. 115–120, Cambridge, MA, 1998.

Korn, J. and Schamel, H., Adiabatic growth of generalized e-holes in drifting plasmas, *Phys. Lett., A 208,* 328–334, 1995.

Krasovsky, V. L., Matsumoto, H., and Omura, Y., Bernstein-Greene-Kruskal analysis of electrostatic solitary waves observed with Geotail, *J. Geophys. Res., 102,* 22,131–22,139, 1997.

Lynov, J.P., Michelsen, P., Pecseli, H.L., et al., Observations of solitary structures in a magnetized, plasma loaded waveguide, *Physica Scripta, 20,* 328–335, 1979.

Matsumoto, H., Kojima, H., Miyake, T., et al., Electrostatic solitary waves (ESW) in the magnetotail: BEN wave forms observed by GEOTAIL, *Geophys. Res. Lett., 21,* 2915–2918, 1994.

Miyake, T., Omura, Y., Matsumoto, H.,and Kojima, H., Two-dimensional computer simulations of electrostatic solitary waves observed by Geotail spacecraft, *J. Geophys. Res., 103,* 11,841–11,850, 1998.

Morse, R. L. and Nielson C. W., One-,two-,and three-dimensional numerical simulation of two-beam plasmas, *Phys. Rev. Lett., 23,* 1087–1090, 1969.

Mozer, F.S., Ergun, R.E., Temerin, M., et al., New features of time domain electric-field structures in the auroral acceleration region, *Phys. Rev. Lett., 79,* 1281–1284, 1997.

Muschietti, L., Roth, I., and Ergun, R. E., On the formation of wave packets in planetary foreshocks, *J. Geophys. Res., 101,* 15,605–15,613, 1996.

Muschietti, L., Ergun, R. E., Roth, I., and Carlson, C. W., Phase-space electron holes along magnetic field lines, *Geophys. Res. Lett., 26,* 1093–1096, 1999a.

Muschietti, L., Ergun, R. E., Roth, I., and Carlson, C. W., Correction to "Phase-space electron holes along magnetic field lines", *Geophys. Res. Lett., 26,* 1689, 1999b.

Omura, Y., Matsumoto, H., Miyake, T., and Kojima, H., Electron beam instabilities as generation mechanism of electrostatic solitary waves in the magnetotail, *J. Geophys. Res., 101,* 2685–2697, 1996.

Saeki, K., Michelsen, P., Pecseli, H.L., and Rasmussen, J.J., Formation and coalescence of electron solitary holes, *Phys. Rev. Lett., 42,* 501–504, 1979.

Saeki, K. and Genma, H., Electron-hole disruption due to ion motion and formation of coupled electron hole and ion-acoustic soliton in a plasma, *Phys. Rev. Lett., 80,* 1224–1227, 1998.

Schamel, H., Theory of electron holes, *Phys. Scr., 20,* 336–342, 1979.

Schamel, H., Stability of electron vortex structures in phase space, *Phys. Rev. Lett., 48,* 481–483, 1982.

Turikov, V. A., Electron phase-space holes as localized BGK solutions, *Phys. Scr., 30,* 73–77, 1984.